Improved tropospheric ozone profile retrievals using OMI and TES radiances

John Worden,[1] Xiong Liu,[2] Kevin Bowman,[1] Kelly Chance,[2] Reinhard Beer,[1] Annmarie Eldering,[1] Michael Gunson,[1] and Helen Worden[1]

Received 7 August 2006; revised 9 November 2006; accepted 6 December 2006; published 10 January 2007.

[1] We perform a study for characterizing the vertical resolution of tropospheric ozone profile retrievals from the combination of simulated ultraviolet (UV) and thermal infrared (TIR) observations that are representative of the EOS Aura Ozone Monitoring Instrument (OMI) and the Tropospheric Emission Spectrometer (TES). Under the low thermal contrast conditions used for this simulation, we find that estimating ozone profiles by combining UV and TIR radiances results in a factor of two or more improvement in the ability to resolve boundary layer ozone, as compared with either instrument alone. In addition, there is a substantial improvement in the vertical resolution of ozone in the free troposphere (between 20% and 60%) as compared to the TES vertical resolution. This study points towards the importance of combining multiple spectral regions for dramatically improving the sounding of tropospheric trace gases. **Citation:** Worden, J., X. Liu, K. Bowman, K. Chance, R. Beer, A. Eldering, M. Gunson, and H. Worden (2007), Improved tropospheric ozone profile retrievals using OMI and TES radiances, *Geophys. Res. Lett.*, *34*, L01809, doi:10.1029/2006GL027806.

1. Introduction

[2] Vertically resolved estimates of tropospheric ozone are critical towards understanding the distinct roles that ozone plays in different parts of the atmosphere. For example, ozone is a greenhouse gas in the upper troposphere, an atmospheric cleanser in the middle troposphere and is a major component of photochemical smog in the boundary layer [e.g., *Jacob*, 1999, and references therein]. In particular, direct measurements of boundary layer ozone formation are necessary for understanding ozone formation in polluting regions and its subsequent venting into the free troposphere [*Agustí-Panareda et al.*, 2005; *Auvray and Bey*, 2005]. Ozone vented from the boundary layer or chemically formed in the free troposphere can then be globally transported because the lifetime of ozone in the middle and upper troposphere is on the order of weeks to months. This free-tropospheric ozone can then subside into the boundary layer where it can add significantly to the local pollution burden [e.g., *Guttikunda et al.*, 2005]. Vertically resolved estimates of boundary layer and the free tropospheric ozone are therefore critical towards understanding these ozone sources and processes.

[3] The Ozone Monitoring Instrument (OMI) and the Tropospheric Emission Spectrometer (TES) instruments, launched in July 2004 on the EOS Aura satellite, both estimate tropospheric ozone from nadir (downward looking) measurements of ultraviolet (UV) and thermal infrared (TIR) radiances respectively. The OMI instrument can obtain measurements of tropospheric ozone with ~12 km vertical resolution with global sampling and a footprint of 13 km by 48 km at nadir. The TES measurements yield much less horizontal coverage (about 1 profile every 2.2° latitude along each of the 16 orbits in one day); however the TES measurements provide vertically resolved estimates of tropospheric ozone with a vertical resolution of about 6 km. A weakness of both of these instruments is the general inability to resolve the boundary layer ozone for typical atmospheric conditions, except in the summer when TES ozone estimates are sensitive to boundary layer ozone where the surface temperature is over 300 K and there is significant (larger than 10 K) thermal contrast between the ground and air.

[4] Here we show the predicted characterization of ozone profile estimates if OMI and TES radiances are simultaneously used for estimating ozone. The advantages of combining these measurements through an optimal estimation algorithm are a dramatic (factor of 2 or more) improvement in the sensitivity to boundary layer and free tropospheric ozone as compared to just using the thermal infrared. This study involving simulated ozone estimates is a necessary pre-requisite for beginning the task of combining these observations and the corresponding forward models, and staging them on a computer cluster capable of producing a significant number of ozone estimates.

2. Description of OMI and TES

[5] Observations with moderate spectral resolution and high signal to noise ratio in the Hartley and Huggins UV ozone absorption bands provide vertical information of ozone, including the troposphere, due to the wavelength dependent photon penetration resulting from the wavelength-dependent ozone absorption and Rayleigh scattering and due to the temperature-dependent ozone absorption Huggins bands [*Chance et al.*, 1997]. This has been demonstrated from GOME observations [*Munro et al.*, 1998; *Liu et al.*, 2005, 2006]. OMI is a nadir-viewing imaging spectrograph that takes measurements of the backscattered solar radiation from the Earth's atmosphere and surface in the ultraviolet and visible region (270–500 nm) with a spectral resolution of 0.42 – 0.63 nm. It measures total column ozone, ozone profile, and other trace gases

[1]Earth and Space Sciences Division, Jet Propulsion Laboratory, Pasadena, California, USA.
[2]Atomic and Molecular Physics Division, Harvard-Smithsonian Center for Astrophysics, Cambridge, Massachusetts, USA.

0094-8276/07/2006GL027806$05.00

(e.g., NO_2, HCHO, SO_2, BrO, OClO, CHOCHO) as well as UV-absorbing aerosols and clouds. The spatial resolution is normally 13 km along-track × 48 km across-track at nadir for UV-1 channel (270–310 nm) and 13 × 24 km^2 for UV-2 (310–365 nm) and visible (365–500 nm) channels. It provides daily global coverage with a full swath width of ~2600 km [*Levelt et al.*, 2002].

[6] TES [*Beer et al.*, 2001] provides a global view of tropospheric trace gas profiles including ozone, water vapor, and carbon monoxide along with atmospheric temperature, surface temperature and emissivity, and an estimate of effective cloud top pressure and an effective optical depth. These observations are important for understanding global air quality and climate.

[7] TES is an infrared, high resolution, Fourier Transform spectrometer covering the spectral range between 650 to 3050 cm^{-1} (3.3 to 15.4 μm) at an apodized spectral resolution of 0.1 cm^{-1} for the nadir viewing and 0.025 cm^{-1} for the limb viewing mode. Spectral radiances measured by TES are used to infer the atmospheric profiles through a non-linear optimal estimation algorithm that minimizes the difference between these radiances and those calculated with the equation of radiative transfer subject to the constraint that the parameters are consistent with a statistical a priori description of the atmosphere [*Rodgers*, 2000; *Bowman et al.*, 2006].

3. Description of Case Study

[8] The sensitivity of a thermal IR instrument to boundary layer ozone is critically dependent on the thermal contrast between the surface and the boundary layer. An objective for our study is to examine the sensitivity of a combined OMI and TES retrieval to the free troposphere and boundary layer ozone when the thermal contrast is low because low thermal contrasts are typical throughout most of the year over both land and ocean. For convenience, simulated radiances and Jacobians are calculated using atmospheric temperature, water, surface temperature and emissivity from TES observations during November 2005 that crosses the Caribbean and North America where the thermal contrast is observed to be low in the boundary layer. These calculations also use simulated ozone fields that are taken from the GEOS-CHEM model [e.g., *Bey et al.*, 2001, and references therein]. We chose this particular set of ozone profiles, which vary between 30 PPB and 70 PPB in the boundary layer, in order to test how well the combined UV and IR ozone retrieval captures the spatial variability of ozone.

4. Description of Forward Model and Atmospheric Profile Retrieval

4.1. Forward Model for UV

[9] Radiances and weighting functions in the UV spectral region measured by OMI are simulated using the Linearized Discrete Ordinate Transfer model (LIDORT) [*Spurr et al.*, 2001]. This spectral region includes the ozone Hartley and Huggins bands, i.e., 270–310 nm in UV1 channel and 310–340 nm in UV2 channel sampled at a total of 317 wavelengths. In the version of LIDORT used here, the pseudo-spherical approximation [*Spurr*, 2002] is applied and the effect of polarization on radiances is not considered. We include ozone, aerosols, surface reflection, and Rayleigh scattering in the simulation, which is adequate for this theoretical study. The surface is assumed to be Lambertian, with a surface albedo of 0.03 and 0.065 for land and water surfaces, respectively [*Herman and Celarier*, 1997]. Aerosol loading and aerosol optical properties are taken from LOWTRAN [*Kneizys et al.*, 1988], with maritime (rural) type aerosols (visibility: 23 km) in the boundary layer over ocean (land), and background aerosols in the free troposphere and stratosphere. The aerosol optical thickness is ~0.27 at 550 nm. The viewing geometry is based on OMI observations at nadir that coincide spatiotemporally with TES observations.

4.2. Forward Model for IR

[10] Radiances and weighting functions in the thermal IR spectral region measured by TES are simulated using a code that is based on LBLRTM [*Clough et al.*, 2006]. Clouds are accounted for in TES profile estimates by simultaneously estimating an effective optical depth and cloud top pressure [*Kulawik et al.*, 2006]. However, we do not consider clouds in this paper because we are interested in the conditions that will allow Aura measurements to better infer boundary layer ozone. Surface emissivity and temperature are estimated along with all profiles for land scenes, but emissivity is fixed for ocean scenes. The IR spectral regions used for the TES and the TES/OMI ozone estimates are essentially the same as those described by *Worden et al.* [2004]. However, we now combine the IR Jacobians from the 15 μm CO_2 band, the 9.6 μm Ozone band, and several water lines near 1200 cm^{-1} in order to simultaneously estimate temperature, water, ozone, and surface properties for this simulation. This updated strategy is consistent with the approach used by current TES atmospheric profile retrievals.

4.3. Linear Retrieval

[11] For this study we simultaneously estimate ozone, temperature, water, and surface properties by assuming the combination of OMI and TES radiance measurements. Our analysis is then to compare the ozone estimate from combining OMI and TES measurements to those from OMI and TES alone. Synthetic ozone estimates are calculated using the linear retrieval [*Rodgers*, 2000; *Worden et al.*, 2004; *Bowman et al.*, 2006]. If the final estimate is close to the true state, then the estimated ozone can be related to the a priori constraint used in the retrieval and the true ozone profile using the linear relationship:

$$\hat{\mathbf{x}} = \mathbf{x}_c + \mathbf{A}(\mathbf{x} - \mathbf{x}_c) \quad (1)$$

The vector $\hat{\mathbf{x}}$ refers in this study to the synthetic ozone estimate. The vector $\mathbf{x}$ refers to the true state of ozone, which is given by the GEOS-CHEM model fields, and the vector $\mathbf{x}_c$ is the a priori constraint vector which we hold fixed for all synthetic estimates in order to better observe how the different measurement approaches captures the ozone variability. The averaging kernel $\mathbf{A}$, or resolution matrix, is a function of the Jacobian matrix, measurement error covariance, and the constraint matrix. The Jacobian matrix is the sensitivity of the measurement with respect to the estimated parameters which are ozone, temperature,

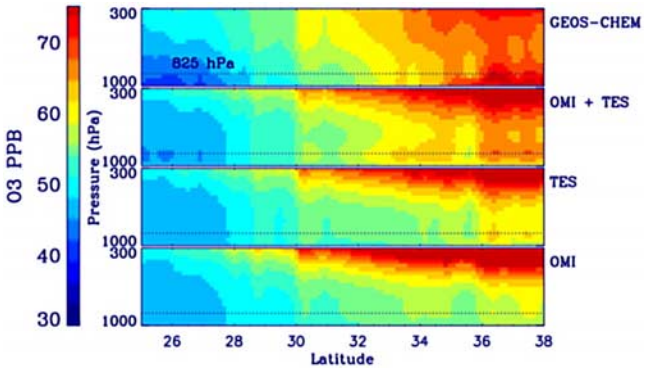

Figure 1. (first panel) A Curtain Plot of the GEOS-CHEM ozone fields used for the study. (second panel) The synthetic estimated ozone using simultaneous measurements from OMI and TES. (third panel) The synthetic estimated ozone using TES infrared radiances. (fourth panel) The synthetic estimated ozone using OMI UV radiances. All ozone profile retrievals use a common a priori constraint that is consistent with the GEOS-CHEM profile shown at 27 degrees latitude. The ocean scenes are south of 30 degrees latitude.

water and surface properties. In order to linearly estimate an ozone profile for a synthetic OMI and TES retrieval, the Jacobians corresponding to each instrument are combined. The constraint matrix is a block-diagonal matrix containing the inverse of the climatological variances for ozone, temperature, water, and the surface terms as described by *Worden et al.* [2004]. The measurement error covariance here is a diagonal value containing the square of the Noise Equivalent Spectral Radiance (NESR) for each measurement. For the synthetic ozone estimates, the averaging kernel matrix in Equation (1) is the block-diagonal component that is associated with ozone. Note that for this study we do not include noise in the profile retrievals, although the measurement covariance is included when calculating the averaging kernel, as we are primarily focused on examining the improved vertical resolution of the free troposphere and boundary layer from combining UV and IR measurements.

[12] The averaging kernel matrix is also used to define the "resolution" of the retrieval. The vertical resolution of an atmospheric retrieval, defined on a pressure (or altitude) grid, can be derived from the rows of the averaging kernel matrix, $\partial \hat{\mathbf{x}}_i / \partial \mathbf{x}$, which define the relative contribution of each element of the true state to the estimate at a particular pressure (or altitude). The resolution can be defined as the full-width-half-maximum of the rows of the averaging kernel. The averaging kernel matrix is also used to compute the number of degrees of freedom for signal (DOFS) of the retrieval [*Rodgers*, 2000], defined as

$$\mathrm{DOFS} = \mathrm{tr}[\mathbf{A}_{xx}]. \quad (2)$$

DOFS may be interpreted as the number of statistically independent elements of the estimate. A value of zero for any diagonal element of the averaging kernel implies that the corresponding parameter is insensitive to the true state. A value of 1 implies the estimated parameter will completely capture any variability of this parameter. We therefore use the DOFS value as a measure of the sensitivity of the estimated ozone at one or more levels of the atmosphere such as the boundary layer.

5. Results

[13] In order to show how combining TES and OMI radiances results in improved tropospheric ozone estimates, Figure 1 shows an image of the vertical ozone distributions from the GEOS-CHEM, as well as the estimates assuming TES-only and OMI-only observations along with ozone estimate if TES and OMI observations are combined.

[14] The a priori constraint used for all of the estimated ozone profiles in Figure 1 is equivalent to the GEOS-CHEM ozone field at 27 degrees latitude. The level at 825 hPa is indicated by a dotted line and is used as a proxy for the top of the boundary layer. The ocean scenes are all south of 30 degrees latitude. Although there is improved sensitivity to boundary layer ozone over the ocean, the greatest improvement is over land. For example, the GEOS-CHEM ozone at 900 hPa at 35 degrees latitude is 60 PPB. The a priori ozone at this pressure is 43 PPB. The estimate from a simulated OMI/TES profile retrieval also gives about 60 PPB whereas the estimates from and OMI alone and TES alone retrieval is about 50 PPB. While this agreement is poorer at other latitudes, the combined OMI/TES profile retrieval substantially improves the accuracy of the estimate over a much wider latitudinal range than OMI or TES alone. The combined OMI/TES retrieval also better captures the horizontal and vertical variability of ozone in the free troposphere up to about 300 hPa as indicated in Figure 1. However, there is only marginal improvement in the estimated upper tropospheric ozone using the combined retrieval. The larger ozone values in the upper troposphere, as compared to the GEOS-CHEM values result from the coarse vertical resolution of the estimate in the upper troposphere and lower stratosphere. As shown in Equation (1), coarse vertical resolution will propagate differences between the "true" and a priori ozone in the lower stratosphere to the upper troposphere.

[15] The improved vertical resolution to tropospheric ozone is interpreted in Figure 2 in which we show an example of the averaging kernels for the OMI-only, TES-only, and OMI + TES results for the ozone estimate at 30.5 degrees latitude. Both OMI and TES estimates are sensitive to tropospheric ozone. For this case, TES shows little sensitivity to the boundary layer ozone but can better resolve the lower troposphere and upper troposphere from the stratosphere. All of the OMI averaging kernels peak at around 700 hPa but it is challenging to distinguish this tropospheric amount from the stratospheric ozone because the tropospheric averaging kernels have cross-terms in the stratosphere that are of similar magnitude. However a significant feature of the OMI averaging kernels is that they are all slightly sensitive to the boundary layer. Consequently, when TES observations, which can vertically resolve the free troposphere, and OMI observations, which are sensitive to the boundary layer, are combined, the resulting estimate shows a increased sensitivity to boundary layer ozone.

[16] Figure 3 shows the improvement in sensitivity to ozone across the oceanic and land scenes that compose this transect. We calculate the DOFS between the surface and

825 hPa as a metric for the sensitivity of the ozone estimate to boundary layer ozone. The top panel of Figure 3 shows the DOFS for the boundary layer. The sensitivity improvement ranges from 30% over the ocean scenes to almost a factor of 4 over the land where there is more ozone, as well as increased thermal contrast, and enhanced reflectivity of the UV. The increased vertical resolution is particularly striking near 34 degrees latitude. At this latitude, the TES averaging kernel is strongly peaked in the middle and upper troposphere and is negligible in the lower troposphere and boundary layer, whereas the OMI averaging kernels have peak sensitivity below the altitude where the TES ozone estimate is most sensitive. Consequently, the combination of TES and OMI better distinguishes the boundary layer ozone. This situation where the TES and OMI averaging kernels are more separated changes just north of 34 degrees in which the OMI and TES averaging kernels more strongly overlap because of changing atmospheric thermal conditions and solar zenith angle and consequently the sensitivity to boundary layer ozone reduces. The middle panel of Figure 3 shows the DOFS for the region between the surface and 100 hPa; the improvement in vertical resolution for this set of land and ocean scenes ranges between 20% and 60%. As discussed earlier, most of this improvement is in the free troposphere below 300 hPa; this is the region where TES and OMI averaging kernels show the greatest sensitivity to tropospheric ozone. The bottom panel shows the fractional difference between the "true" (GEOS-CHEM) ozone fields and the estimates from the different measurement approaches. As expected, the fractional difference is smallest where the sensitivity is largest.

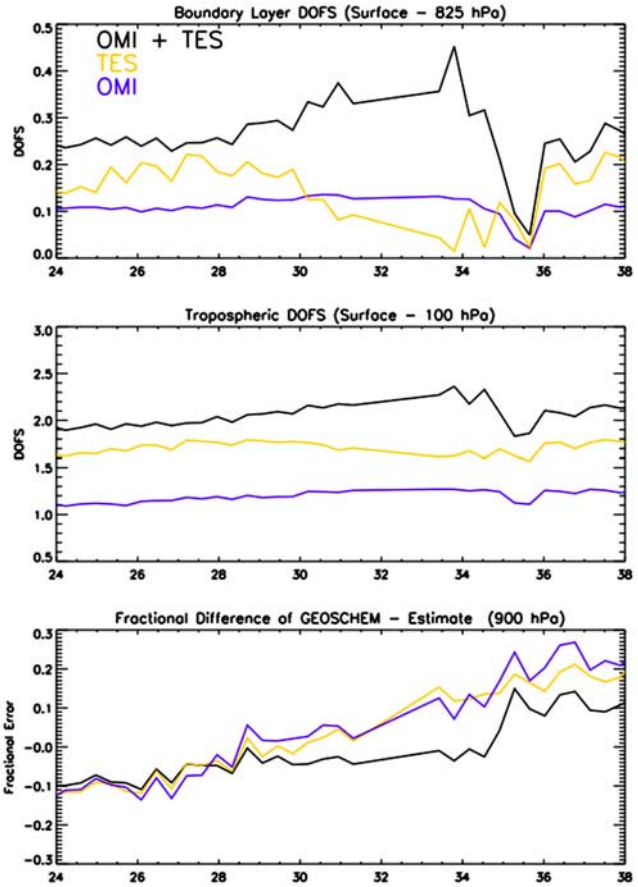

Figure 3. (top) The boundary layer DOFS for the set of ozone profiles in Figure 1 as would be measured by OMI (purple line), TES (orange line) and OMI plus TES (black line). (middle) The total DOFS for the region between the surface and 100 hPa. (bottom) The fractional difference at 900 hPa between the simulated "true" GEOS-CHEM ozone profiles and the simulated estimates from the different measurement approaches.

6. Discussion and Conclusions

[17] We show in this study that combining OMI (UV) and TES (IR) radiance measurements allows for a dramatic improvement (between 30% to 400%) in the vertical resolution of ozone estimates in the boundary layer as well as a substantial improvement (30% to 60%) in the free troposphere. This increased sensitivity results from the vertical resolution in the troposphere provided by high-resolution (0.1 cm^{-1}) IR measurements combined with sensitivity to the boundary layer provided by UV radiance measurements.

[18] Future missions which use combined UV and IR measurements to determine boundary layer O_3 will likely also employ measurements in the visible. Measurements in the visible Chappuis bands have averaging kernels that are almost constant in height, down to ground or cloud-top level, as opposed to the UV and IR averaging kernels, which peak above the boundary layer. The use of visible measurements will thus enhance the ability to measure O_3 in the boundary layer and surface and distinguish it from O_3 higher in the troposphere [*Chance et al.*, 1991, 1997].

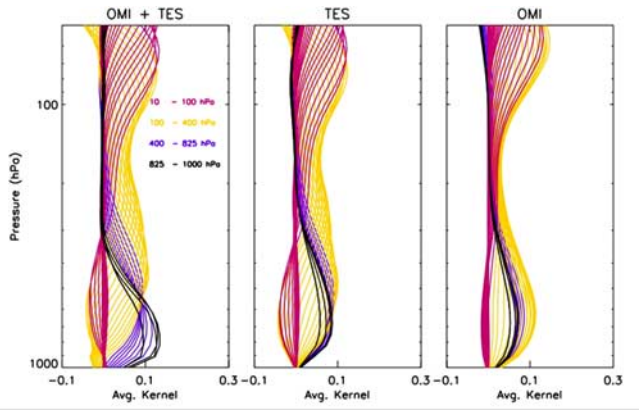

Figure 2. Examples of averaging kernels. (left) Averaging kernels for an OMI and TES synthetic ozone profile retrieval for the ozone estimate at 30.5 degrees latitude shown in Figure 1. (middle, right) Averaging kernels for this same scene but assuming a TES and OMI sounding of this scene, respectively.

[19] **Acknowledgments.** The research described in this paper was carried out at the Jet Propulsion Laboratory, California Institute of Technology, under a contract with the National Aeronautics and Space Administration. Research at the Smithsonian Astrophysical Observatory was supported by the National Aeronautics and Space Administration and by the Smithsonian Institution. We are grateful for ongoing encouragement from the OMI Principal Investigator and the U.S. and international OMI Science Teams.

References

Agustí-Panareda, A., S. L. Gray, and J. Methven (2005), Numerical modeling study of boundary-layer ventilation by a cold front over Europe, *J. Geophys. Res.*, *110*, D18304, doi:10.1029/2004JD005555.

Auvray, M., and I. Bey (2005), Long-range transport to Europe: Seasonal variations and implications for the European ozone budget, *J. Geophys. Res.*, *110*, D11303, doi:10.1029/2004JD005503.

Beer, R., T. A. Glavich, and D. M. Rider (2001), Tropospheric Emission Spectrometer for the Earth Observing System's Aura satellite, *Appl. Opt.*, *40*, 2356–2367.

Bey, I., D. J. Jacob, R. M. Yantosca, J. A. Logan, B. D. Field, A. M. Fiore, Q. Li, H. Y. Liu, L. J. Mickley, and M. G. Schultz (2001), Global modeling of tropospheric chemistry with assimilated meteorology: Model description and evaluation, *J. Geophys. Res.*, *106*, 23,073–23,095.

Bowman, K. W., et al. (2006), Tropospheric emission spectrometer: Retrieval method and error analysis, *IEEE Trans. Geosci. Remote Sens.*, *44*, 1297–1307.

Chance, K. V., J. P. Burrows, and W. Schneider (1991), Retrieval and molecule sensitivity studies for the Global Ozone Monitoring Experiment and the SCanning Imaging Absorption spectroMeter for Atmospheric CHartographY, *Proc. SPIE Int. Soc. Opt. Eng.*, *1491*, 151–165.

Chance, K. V., J. P. Burrows, D. Perner, and W. Schneider (1997), Satellite measurements of atmospheric ozone profiles, including tropospheric ozone, from UV/visible measurements in the nadir geometry: A potential method to retrieve tropospheric ozone, *J. Quant. Spectrosc. Radiat. Transfer*, *57*, 467–476.

Clough, S. A., et al. (2006), Forward model and Jacobians for Tropospheric Emission Spectrometer retrievals, *IEEE Trans. Geosci. Remote Sens.*, *44*, 1308–1323.

Guttikunda, S. K., Y. Tang, and G. R. Carmichael (2005), Impacts of Asian megacity emissions on regional air quality during spring 2001, *J. Geophys. Res.*, *110*, D20301, doi:10.1029/2004JD004921.

Herman, J. R., and E. A. Celarier (1997), Earth surface reflectivity climatology at 340–380 nm from TOMS data, *J. Geophys. Res.*, *102*, 28,003–28,011.

Jacob, D. J. (1999), *Introduction to Atmospheric Chemistry*, Princeton Univ. Press, Princeton, N. J.

Kneizys, F. X., E. P. Shettle, L. W. Abreu, J. H. Chetwynd, G. P. Anderson, W. O. Gallery, J. E. A. Selby, and S. A. Clough (1988), *Users Guide to LOWTRAN 7*, Air Force Geophys. Lab., Hanscom AFB, Mass.

Kulawik, S., et al. (2006), Implementation of cloud retrievals for Tropospheric Emission Spectrometer (TES) atmospheric retrievals: 1. Description and characterization of errors on trace gas retrievals, *J. Geophys. Res.*, *111*, D24204, doi:10.1029/2005JD006733.

Levelt, P. F., J. P. Veefkind, R. H. M. Voors, and J. de Vries (2002), Instrument description, in *OMI Algorithm Theoretical Basis Document*, vol. 1, *OMI Instrument, Level 0-1b Processor, Calibration & Operations*, edited by P. F. Levelt, pp. 9–10, NASA Goddard Space Flight Cent., Greenbelt, Md.

Liu, X., K. Chance, C. E. Sioris, R. J. D. Spurr, T. P. Kurosu, R. V. Martin, and M. J. Newchurch (2005), Ozone profile and tropospheric ozone retrievals from Global Ozone Monitoring Experiment: Algorithm description and validation, *J. Geophys. Res.*, *110*, D20307, doi:10.1029/2005JD006240.

Liu, X., et al. (2006), First directly-retrieved global distribution of tropospheric column ozone from GOME: Comparison with the GEOS-CHEM model, *J. Geophys. Res.*, *111*, D02308, doi:10.1029/2005JD006564.

Munro, R., R. Siddans, W. J. Reburn, and B. Kerridge (1998), Direct measurement of tropospheric ozone from space, *Nature*, *392*, 168–171.

Rodgers, C. D. (2000), *Inverse Methods for Atmospheric Sounding: Theory and Practice*, World Sci., Hackensack, N. J.

Spurr, R. J. D. (2002), Simultaneous derivation of intensities and weighting functions in a general pseudo-spherical discrete ordinate radiative transfer treatment, *J. Quant. Spectrosc. Radiat. Transfer*, *75*, 129–175.

Spurr, R. J. D., T. P. Kurosu, and K. V. Chance (2001), A linearized discrete ordinate radiative transfer model for atmospheric remote-sensing retrieval, *J. Quant. Spectrosc. Radiat. Transfer*, *68*, 689–735.

Worden, J., et al. (2004), Predicted errors of tropospheric emission spectrometer nadir retrievals from spectral window selection, *J. Geophys. Res.*, *109*, D09308, doi:10.1029/2004JD004522.

R. Beer, K. Bowman, A. Eldering, M. Gunson, H. Worden, and J. Worden, Earth and Space Sciences Division, Jet Propulsion Laboratory, 4800 Oak Grove Drive, MS 183-301, Pasadena, CA 91109, USA. (john.worden@jpl.nasa.gov)

K. Chance and X. Liu, Atomic and Molecular Physics Division, Harvard-Smithsonian Center for Astrophysics, 60 Garden Street, MS-50, Cambridge, MA 02138, USA.